Dynamic modeling of water temperature and flow in large water system

Gautier Hypolite, Jean-Henry Ferrasse, Olivier Boutin, Sandrine del Sole, Jean-François Cloarec

Dynamic modeling of water temperature and flow in large water system

Gautier Hypolite [a,b], Jean-Henry Ferrasse [a,*], Olivier Boutin [a], Sandrine Del Sole [b], Jean-François Cloarec [b]

[a] Aix Marseille Univ, CNRS, Centrale Marseille, M2P2, Marseille, France
[b] Société du canal de Provence, Le Tholonet - CS70064, 13182 Aix-en-Provence Cedex 5, France

ARTICLE INFO

Keywords:
Water temperature
Unsteady heat transfer
Water supply
Soil temperature model

ABSTRACT

Thermal energy counts for a large part of the total energy consumption. To reduce fossil fuel consumption for heat and cold generation, different low temperature heat sources have been considered. Water networks have been considered as a large amount of water flow through it. To measure the thermal potential of the system, this paper provides a method in unsteady state to determine water temperature and flow in large water systems made of buried pipes. The model has been applied to a raw water supply system made up of 5000 km of piping and carrying 200 million m^3 annually situated in the south of France. Water temperature is calculated considering heat exchange and the spatial specificities of the network (diameter of the pipes, depth, type of soil …). Soil and water temperature measurements have been made to validate the model values. The model can predict water flow and temperature according to time with good accuracy: maximal error of 10% on the flow is obtained, the root mean square error on the calculated temperature is $0.84°C$, and the correlation coefficient between the calculated and the measured temperature values is 0.98. The impact of adding several heat (or cold) injections in the system has been evaluated with the model. After a 2 MW heat exchange, the water temperature is increased by at least $1circC$ for 10 km downstream the exchange.

1. Introduction

As part of COP 21, France is committed to reduce its energy consumption by 50% and to increase the share of renewable energy to 32% in 2030. In this context, the reduction of consumption for heating and cooling is essential. To reduce the use of fossil fuels, different low temperature heat sources can be used for heat pump operations. Sewage systems, seawater, groundwater, drinking water, or air can all be used as heat sources [1]. In this paper, the raw water network of "canal de Provence" is studied [2]. Drinking water networks have been considered for heat and cold recovery by Van der Hoek et al. [3]. Especially, the integration of heat pump into district heating networks have been studied in Almere (Netherlands) by Blokker et al. [4], in Wrocław (Poland) by Piotr and Elzbieta [5], in Milan (Italy) by De Pasquale et al. [6] and in Copenhagen (Danemark) by Hubeck and Graudal [7]. These studies explain that water temperature is the key parameter to estimate the thermal potential of the system. Water system thermal behavior has also been studied to prevent excessive temperature [8–10]. In order to preserve water quality, some countries (including France) have a regulation that limit water temperature to $25°C$ [11].

For water temperature calculation, the heat exchange between pipes and the surrounding soil must be evaluated. Most of the studies [4,8,9] assume that the presence of a pipe does not influence the temperature of the surrounding soil (undisturbed soil model). The assumption is made because the residence time of water in the system is higher than the time to reach thermal equilibrium. De Pasquale et al. [6] demonstrate that this assumption leads to an important error on the heat transfer, overestimated by a factor of one hundred. These authors compare two models: the first model uses a shape factor to evaluate the heat exchange between the land surface and the pipe. Shape factors allow to rapidly use existing analytic solutions for steady-state problems. They are given for different cases by Incropera et al. [12] (in this case, a horizontal cylinder buried in semi-infinite medium). The second model is the Krarti-Kreider's model [13]. It considers a layer of soil as lagging around the pipe. In a recent article, Hubeck-Graudal et al. [7] use a similar model for the calculation of soil thermal resistance. They suggest that the development of a transient model for the heat exchange would be a "meaningful improvement". That is why the development of a transient model is proposed in this paper.

* Corresponding author.
E-mail addresses: gautier.hypolite@etu.univ-amu.fr (G. Hypolite), jean-henry.ferrasse@univ-amu.fr (J.-H. Ferrasse), olivier.boutin@univ-amu.fr (O. Boutin), sandrine.delsole@canal-de-provence.com (S. Del Sole), jean-francois.cloarec@canal-de-provence.com (J.-F. Cloarec).

Nomenclature

$\dot{m}$	Mass flow, $kg.s^{-1}$
A, B	Dimensionless parameter, –
A_m	Amplitude, $°C$
Cp	Heat capacity, $J.kg^{-1}.K^{-1}$
D	Pipe diameter, m
f	Darcy friction factor, –
H	Burring depth from soil surface to pipe center, m
h_{vol}	Volumetric enthalpy, $J.m^{-3}$
l	Length, m
Nu	Nusselt number, –
Pr	Prandtl number, –
Q	Water flow rate, $m^3.s^{-1}$
R	Thermal resistance, $K.m.W^{-1}$
Re	Reynolds number, –
S	Source term, W
t	Time, s
v	Water velocity, $m.s^{-1}$
z	Depth, m

Greek symbols

α	Thermal diffusivity, $m^2.s^{-1}$
λ	Thermal conductivity, $W.m^{-1}.K^{-1}$
Λ_0	Shape factor, –
Ω	Dimensionless angular frequency, –
ω	Angular frequency, s^{-1}
Φ	Heat flux per unit of length, $W.m^{-1}$
ϕ	Phase difference, –
ρ	Density, $kg.m^{-3}$
σ	Dimensionless burying depth, –
θ	Dimensionless temperature, –

Superscripts, subscripts

cond	Conduction
conv	Convection
in	Inlet
m	Mean
out	Outer
ref	Reference
soil	Soil
tot	Total
w	Water

Acronyms

FEM	Finite Element Method
LST	Land Surface Temperature
MSX	Epanet Multi-Species eXtension

In the petroleum industry, temperature calculations in buried pipes are also of interest. Some hydrocarbons are heated for transportation to decrease their viscosity and prevent the formation of solids [14,15]. For gas transportation, temperature influences the pressure and the flow rate [16,17]. Steady state shape factors are also used for the calculation of heat transfer for a general case of buried pipelines [18,19]. Barletta et al. [14] propose an unsteady method for oil temperature calculation in a single pipes. This method takes into account the presence of pipes on soil temperature. Assuming a sinusoidal variation of soil temperature and using suitable auxiliary variables, the transient problem is converted into a steady problem. Then, the heat transfer between soil and pipe can be calculated using the shape factor and two tabulated parameters. In this industry, transportation is not done in networks but through single pipes. Thus, only the calculation of the heat exchange is made, the network calculation is not necessary.

A key input parameter in the thermal model is the soil surface temperature. Blokker et al. [8] use a complete energy balance at the soil surface to determine soil surface temperature. Agudelo-Vera et al. [10] use the model presented in [8] with weather forecast to predict water temperature. Oosterkamp et al. [16] investigate the impact of soil surface temperature on heat transfer calculations. The best results are obtained using measured soil surface temperature (also called Land Surface Temperature LST). Comparable results are obtained by using a complete energy balance at the soil surface. However, most of the time the value of LST and complete weather data are not available. Therefore, air temperature is often used as an approximation of LST [6,7].

In this study, the land surface temperature measured by satellite [20,21] is used for the first time as an input parameter for water temperature calculation. The value is derived from the NASA satellites Terra and Aqua [22]. The two satellites are part of the Earth Observing System mission. Each satellite provides two values of LST per day with a spatial resolution of one kilometer. Satellite values are compared to in situ measured data for validation in the chosen area.

The goal of this study is to determine an accurate method to determine the temperature in water networks. The method must correctly describe the transient aspect of the problem, be based on a minimum number of measurements, and be easily applicable to any water systems. This article details the modeling of water flow and temperature in water supply systems. The method has been applied to the raw water system of "canal de Provence" in the south of France. The system carries water from the alps to the south east of France, and is situated in the countryside. It is made of 5 000 km of buried pipes that carry 200 million cubic meters of raw water annually [2] (the study was done over 15 000 pipes and 17 000 nodes). Water temperature is obtained by coupling a heat transfer model, hydraulic and thermal solving, and meteorological data under transient conditions. As said before, one of the novelties of this article is to consider the transient state, for that the method of Barletta et al. is integrated to a network calculation.

2. Materials and methods

The originality of the method which is developed is to solve heat and mass conservation on extended water system, taking into account the transient aspect of the heat transfer.

2.1. Thermal model

Water temperature is obtained by solving heat and mass balance into pipes (eq. (1)) and at pipes junctions (eq. (2)).

$$\frac{\partial h}{\partial t} = -v\frac{\partial h}{\partial x} + \frac{4}{\pi\rho D_{in}^2}\cdot\Phi(t) \tag{1}$$

$$h^i = \frac{\sum_j Q_j h^j + S \Big/ \rho}{\sum_j Q_j} \tag{2}$$

Where h is the water specific enthalpy, ρ the water density, D_{in} the inlet diameter of the pipe and Φ the heat flux per unit of length from the surrounding soil to the pipe. i and j respectively refer to flow leaving and entering the node. Q is the water volumetric flow rate and S a source term that can be used to model heat exchange on the network. First, the value of S is set to zero.

Transport calculation is presented with a Lagrangian time based approach [23]. Therefore for a given fluid parcel in the flow, eq. (1)

becomes eq. (3).

$$\frac{dh}{dt} = \frac{4}{\pi\rho D_{in}^2}\cdot\Phi(t) \tag{3}$$

The calculation of heat transfer between the pipe and the surrounding soil is a transient problem as the soil temperature varies according to the season as well as the time of day. $\Phi(t)$ cannot be determined through analytical solution, it is necessary to model these flux variations. The heat flux per unit of length is given in eq. (4). The methods for heat flux calculations are presented in Section 2.1.2.

$$\Phi(t) = \frac{T_\infty(t) - T_w(t)}{R_{tot}(t)} \tag{4}$$

with R_{tot} the total thermal resistance, T_∞ a reference temperature, and T_w the water temperature (the reference temperature depends on the model). The volumetric enthalpy of water is given by (5).

$$h = Cp\cdot(T_w - T_{ref}) \tag{5}$$

By substituting T_w from eq.(5) and (4) into (3) one obtains eq. (6), with parameters given in eq. (7).

$$\frac{dh}{dt} = a\cdot h + b \tag{6}$$

$$\begin{aligned} a &= \frac{-4}{\pi\cdot\rho\cdot Cp\cdot D_{in}^2\cdot R_{tot}} \\ b &= \frac{-4\cdot(T_{ref} - T_\infty)}{\pi\cdot D_{in}^2\cdot R_{tot}} \end{aligned} \tag{7}$$

In this case, a and b are constant on a given hydraulic time step of length Δt. Then the problem given in eq. (6) is a first order linear differential equation that can be solved analytically (eq. (8)).

$$h(t+\Delta t) = \left(h(t) + \frac{b}{a}\right)\cdot\exp(a\cdot\Delta t) - \frac{b}{a} \tag{8}$$

2.1.1. Water temperature calculation

For each time step, the calculation is made by first computing the evolution of enthalpy according to time. Then the transportation in the pipes is determined and then heat and mass balances at the nodes are solved. The evolution of the tracked parameter according to time is specified as a set of Differential–Algebraic Equations (DAE) (in this case eq. (6) and (7)).

As in [6–9], the model equations are solved with the software Epanet MSX (Multi-Species eXtension) [24]. Epanet [25] is an open source software, largely used for hydraulic calculations in water systems. The Lagrangian model from [23] is used by MSX to track the variables into the network. The evolution of volumetric enthalpy is computed using eq. (8). Modifications on the Epanet MSX source code have been made to allow to directly solve this problem instead of a numerical method. The direct solving of the differential equation instead of a numeric method allows to improve accuracy and speeds up the calculation.

2.1.2. Heat transfer model

To compute the value of heat transfer between soil and pipes (value of $\Phi(t)$ in eq. (1)), five models are compared:

- Undisturbed soil model
- Shape factor model
- Krarti-kreider's model
- Numerical model (finite element method)
- Barletta's method

The first four models can be found in [6] and the last one is presented in [14]. For all these models, the input data is the land surface temperature that can be written as a Fourier series (eq (9)).

$$T_{soil}(t,0) = T_m + \sum_{n=1}^{N} a_n \sin(n\omega t + \phi_n) \tag{9}$$

By solving the heat equation in soil, the temperature at the depth z in the soil without pipe is given by eq. (10).

$$T_{soil}(t,z) = T_m + \sum_{n=1}^{N}\left[a_n\cdot\exp\left(-\sqrt{\frac{n\omega}{2\alpha_{soil}}}\cdot z\right)\cdot\sin\left(n\omega t + \phi_n - \sqrt{\frac{n\omega}{2\alpha_{soil}}}\cdot z\right)\right] \tag{10}$$

2.1.2.1. Undisturbed soil model.

The assumption of this model is that the soil temperature is not influenced by the presence of the pipe. Thermal resistance is computed assuming a steady state. The temperature of the pipe's outer wall is equal to the temperature of the soil at the buried depth (eq. (11)).

$$T_\infty(t) = T_{soil}(t,H) \tag{11}$$

The total thermal resistance (eq. (12)) is the sum of two terms accounting for convection inside the pipe (eq. (13)) and conduction (eq. (14)) through the pipe wall.

$$R_{tot} = R_{conv} + R_{cond} \tag{12}$$

$$R_{conv} = \frac{1}{\pi D_{in} h_{conv}} \tag{13}$$

$$R_{cond} = \frac{\ln(D_{out}/D_{in})}{2\pi\lambda_{pipe}} \tag{14}$$

The convection heat transfer is obtained with the Nusselt number and the Gnielinski correlation [12].

2.1.2.2. Shape factor.

Assuming a steady conduction between the soil surface and the pipe, another approach is to use a shape factor [7,18,19]. Incropera et al. [19] give the shape factor for steady-state conduction between a cylinder buried in a semi-infinite medium and the surface (eq. (15)).

$$\Lambda_0 = \frac{2\pi}{acosh\left(\frac{2H}{D_{out}}\right)} \tag{15}$$

Where H is the buried depth of the pipe (distance between the soil surface and the pipe center). The total thermal resistance is given by eq. (16).

$$R_{tot} = R_{conv} + R_{cond} + \frac{1}{\lambda_{soil}\Lambda_0} \tag{16}$$

The reference temperature is the soil surface temperature ($T_\infty = T_{soil}(t, 0)$).

2.1.2.3. Krarti-Kreider.

For the calculation of heat flux between water pipe and soil, De Pasquale et al. [6] use a model developed by Krarti and Kreider [13]. The model was first made for the calculation of heat exchange between air pipe and soil with a daily variation. In this model, a layer of soil around the pipe is considered as lagging. The layer thickness l is given by eq. (17). The model is valid when the layer thickness is small compared to the buried depth [13].

$$l = \sqrt{\frac{\alpha_{soil}}{\omega}} \tag{17}$$

With α_{soil} the soil thermal diffusivity and ω the angular frequency of the

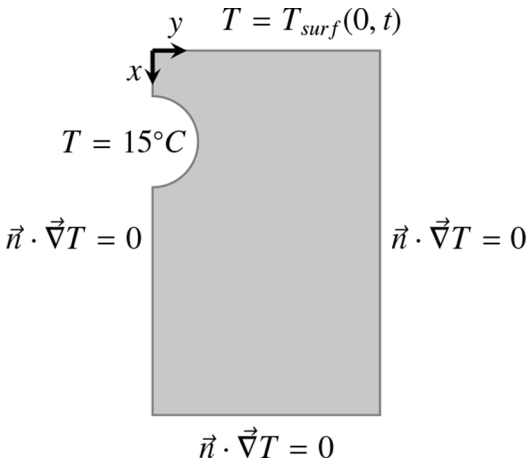

Fig. 1. Calculation domain with boundary conditions.

periodic variation (the period is one year). ω is given by eq. (18).

$$\omega = 1.991 \cdot 10^{-7} rad.s^{-1} \tag{18}$$

For a typical value of soil thermal diffusivity $\alpha_{soil} = 7 \cdot 10^{-7} m^2.s^{-1}$, the layer thickness is $l = 1.88m$. This value is higher than the pipes diameter and the buried depth, therefore the hypothesis on the thickness is not valid.

The temperature at the pipe buried depth is taken as the reference temperature ($T_\infty = T_{soil}(t, H)$) and thermal resistance is given by eq. (19).

$$R_{tot} = R_{conv} + R_{cond} + \frac{\ln(\frac{D_{out}+l}{D_{out}})}{2\pi\lambda_{soil}} \tag{19}$$

2.1.2.4. Finite element method. As a reference, the heat transfer is solved with a transient numerical method. The calculation is performed using a finite element method as in the studies [14,6]. The heat equation is solved in a plane orthogonal to the pipe. The computational domain and the boundary conditions are shown on Fig. 1. The size of the computational domain is 10 m by 10 m. The calculation is simplified by considering only the right half of the plane with a symmetric condition (null heat transfer) on the left boundary. The water temperature in the pipe ($15°C$) is given as boundary condition and the thermal resistances are specified (convection at the inner surface plus conduction through the pipe wall). The land surface temperature (eq. (9)) is specified as the top boundary condition. The bottom condition is assumed adiabatic as the temperature at this depth (10 m) does not vary with time. The influence of pipes on soil temperature can be seen up to 3 m around the pipe. Therefore, temperature is not influenced on the right boundary and the boundary can be considered adiabatic. The calculation is made using Matlab partial differential equation toolbox. Matlab solver is based on a 2D finite element method.

2.1.2.5. Barletta's method. The method was developed in order to calculate the heat flux between the soil and a buried pipeline, assuming a sine variation for the soil surface temperature. Barletta et al. [14] give a method that transforms the transient resolution into a steady one (see appendix 1). If the first harmonic of eq. (9) is considered, the variation of land surface temperature as a function of time is given by eq. (20).

$$T_{soil}(t,0) = T_m + A_m \cdot sin(\omega t + \phi) \tag{20}$$

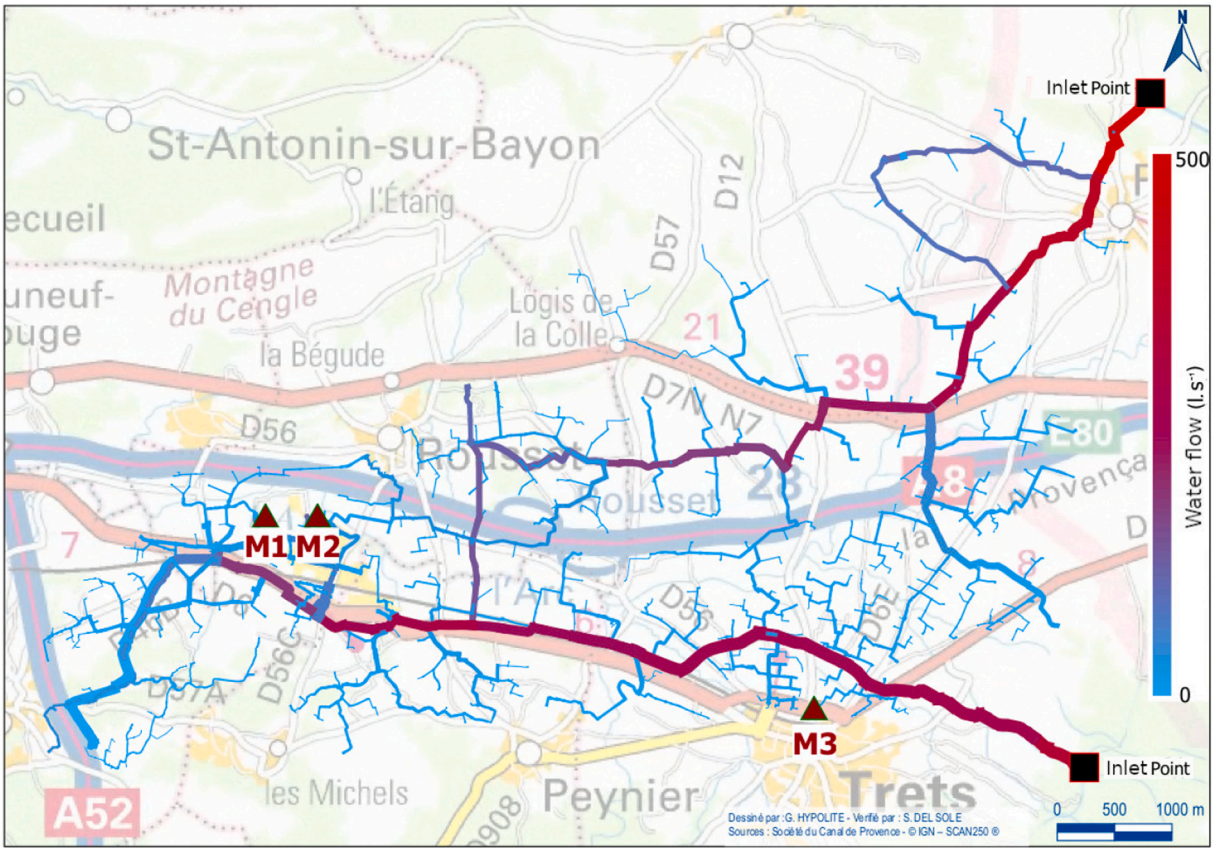

Fig. 2. Raw water system layout, colored according to water flow on the 30rd of June 2018; size of link is proportional to pipe diameter; the network is located at the north east of Marseille. With water temperature measurement position: M1 to M3 (water temperature is also measured at inlet points).

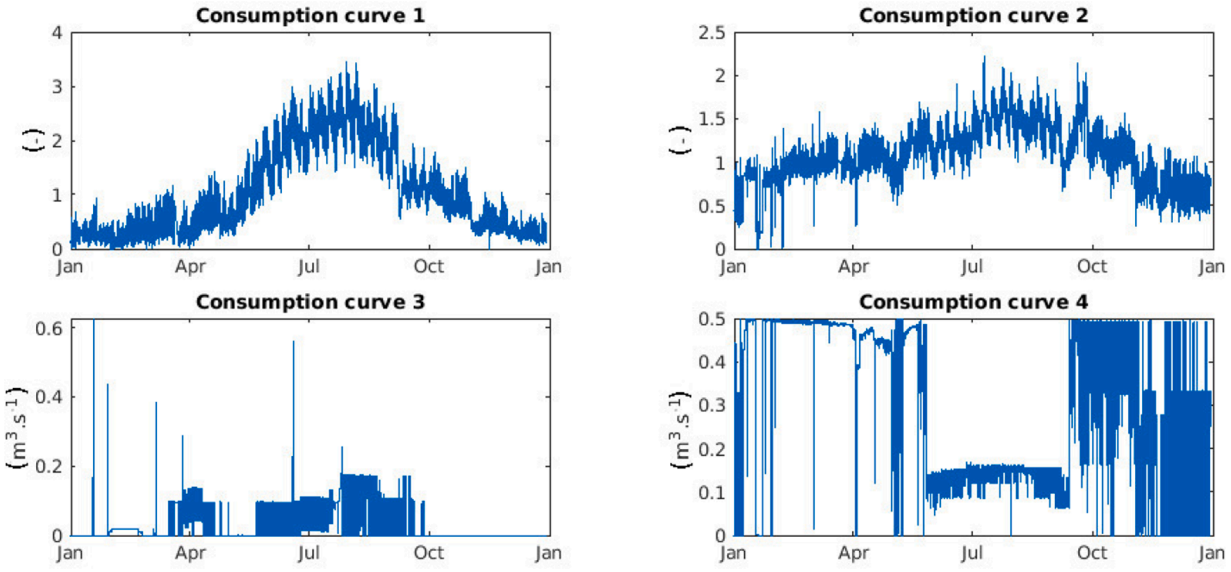

Fig. 3. Pattern for water consumption according to the type of customers, pattern 1 for watering and 2 for domestic use, pattern 3 and 4 for customers equipped with flowmeter (large consumption).

With T_m the mean annual temperature, A_m the amplitude of the oscillation, and ω the angular frequency corresponding to a period of one year (eq. (18)).

The heat flux per unit length between the soil and the outer wall of the pipe is then calculated eq. (21).

$$\Phi(t) = -\lambda_{soil}\cdot\Lambda_0\cdot\left[\left(T_{pipe}^{out} - T_m\right) + A_m\cdot(A\cdot\sin(\omega t+\phi) + B\cdot\cos(\omega t+\phi))\right] \tag{21}$$

Where Λ_0 is the shape factor given in eq. (15). A and B are from the method of Barletta et al. [14] (see appendix). These factors can be tabulated as they only depend on the two parameters given in eq. (22) and (23).

$$\Omega = \frac{\omega D_{out}^2}{4\alpha_{soil}} \tag{22}$$

$$\sigma = \frac{2H}{D_{out}} \tag{23}$$

The pipes are buried so that the top of the pipe is one meter deep. Therefore, for a given conductivity, Ω and σ depend only on the pipes radius as well as A and B. By rearranging eq. (21) with the parameter γ of eq. (24) and considering conduction through the pipe wall, one obtains eq. (25).

$$\gamma(t) = A\cdot\sin(\omega t+\phi) + B\cdot\cos(\omega t+\phi) \tag{24}$$

$$\Phi = \frac{T_m - \gamma(t)\cdot A_m - T_w}{R_{cond} + R_{conv} + 1/(\lambda_{soil}\Lambda_0)} \tag{25}$$

The total thermal resistance is the same as in the shape factor model (eq. (16)) and the reference temperature is given by eq. (26).

$$T_\infty = T_m - \gamma(t)\cdot A_m \tag{26}$$

The reference temperature depends on the pipe diameter. For this reason, the reference temperature must be calculated as a function of time. The implementation of this method into MSX enables the description of the transient aspect of the heat transfer.

2.2. Hydraulic model

A hydraulic model that described water flow and pressure for extended periods is developed on a subpart of the entire network. It is made of 205 km of pipes with two inlet points and is located at the northeast of the city of Marseille (see Fig. 2). It has two inlet points and five temperature measurement points.

The input data are extracted from the network monitoring. The available measurements from the network are:

- Hourly flow and pressure measurements at the inlet and key points on the network,
- Hourly water level in tank,
- Hourly flow measurement for clients with large consumption,
- Annual water consumption for each client.

The structure of the network is given as a set of pipes and nodes (length, diameter, material, and position of pipes are known). Nodes represent the junction between pipes, tanks, inlets of the network and the consumption points.

Water consumption is given according to time for different kinds of consumers (see Fig. 3). For domestic and watering use, there is no flowmeter at the delivery station. The consumption curve 1 and 2 are for watering and domestic use respectively (they show the normalized share of the annual demand). The system shown in Fig. 2 includes 800 watering delivery points for a consumption of 3,125,000 m^3 and 2224 domestic delivery points for a consumption of 1,250,000 m^3 in 2018. For watering use the consumption is high during summer when crops need to be irrigated.

The industrial customers with a significant consumption are equipped with flowmeter. Therefore, the consumption curves are made of measured value (curves 3 and 4 of Fig. 3 are two examples).

2.3. Temperature measurement

2.3.1. Soil temperature measurement

The heat transfer model needs the soil surface temperature as an input. Unlike air temperature, this temperature is not widely monitored. Land Surface Temperature (LST) can be assumed to be equal to the air temperature. An energy balance can be done at the land surface, but a large number of parameters are needed (air temperature, solar

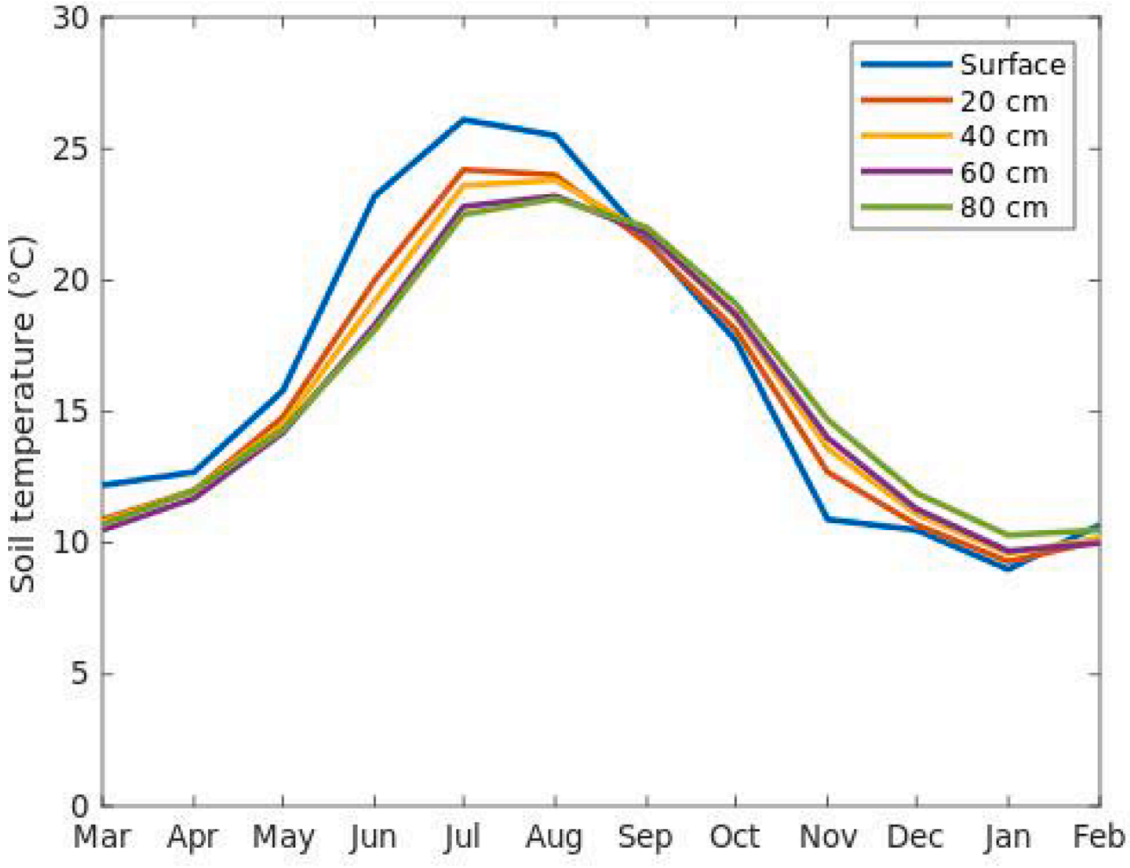

Fig. 4. Measured soil temperature between the surface and 80 cm deep: monthly mean in 2019–2020.

radiation, wind velocity, albedo). All of these parameters are not known in most cases. In this study, satellite measurements are used and validated with in situ measurements. The water system of "canal de Provence" is mainly situated in non-urban area. Therefore, the field cover is mostly natural.

In situ measurements have been made to evaluate the land surface temperature and the thermal diffusion in the soil around a pipe. Two probes were installed, one above a pipe and one at 5 m in the plane orthogonal to the pipe (diameter 800 mm). Measurements are made each 10 cm between the surface and the depth of 80 cm (nine temperature sensors). At 5 m, the soil temperature is not influenced by the presence of the pipe. This probe is used to evaluate the soil behavior without a pipe, particularly the soil thermal diffusivity.

Soil surface temperature varies according to the time of day and the season. The daily variation of temperature is absorbed at a depth of 30 cm. Below this depth, it is possible to conclude that only the seasonal variations have an impact. Fig. 4 shows the monthly mean of soil temperature. Due to thermal conduction in soil, the amplitude of soil temperature variation is reduced with depth and a phase shift appears.

The satellites Terra and Aqua of the Earth Observing System program (EOS) provide dailies values of LST. In the place of interest, the measurements are made at 11 am and 10 pm for the Terra satellite and 1 pm and 2 am for the Aqua satellite (the hour is given in solar time). The history for the measurement since the year 2000 with a spatial resolution of 1 km is available on-line [20,21].

LST has been validated in several places around the world [26]. The satellite measurements for the given location, are compared to in situ measurements. The correlation coefficient of $r^2 = 0.91$ indicates that satellite values are in good agreement with in situ values. Therefore, the satellite measurements are able to describe the variation of LST according to time (day measurement catch the maximum value and night the minimum, the time series for satellite and in situ measurements can be found in the supplementary material).

A Fourier transform is used to fit a sine function with the LST measurement history [27–29]. As the soil temperature at 1 m depth has no daily variation, only the first harmonic of the Fourier transform is used. The values are the upper boundary conditions for the heat transfer in the soil. Fig. 5 shows the satellite measurement of LST for the past ten years in the south of France (city of Toulon). The approximation is calculated with a Fourier transform, which coefficients (eq. (9) and (20)) are $T_m = 17.21°C; A_m = 9.80°C; \omega = 1.991{\cdot}10^{-7}$; $\phi = 2.82$. It can be noticed that the angular frequency value, obtained with the Fourier transform on measured data, exactly correspond to a period of one year ((18)).

2.3.2. *Water temperature measurement*

Water temperature measurements are monitored on the network in order to validate the model. The measurements are made at inlet points and at some water delivery stations in the network of Fig. 2 (points M1, M2, and M3).

3. Results and discussions

3.1. *Hydraulic*

The calculation has been made for years 2017 and 2018 for the water system shown in Fig. 2. Demands for consumers are given with one hour time step. Pipe roughness is determined using pressure measurement on the network. In order to validate the hydraulic model, the calculated inlet flow (eq. (27)) is compared to the measured one. The water flow at the system inlet point is compared to the calculated value. The correlation coefficient over the 17520 measurements is $r^2 = 0.96$. Therefore, the distribution of consumption over time is validated.

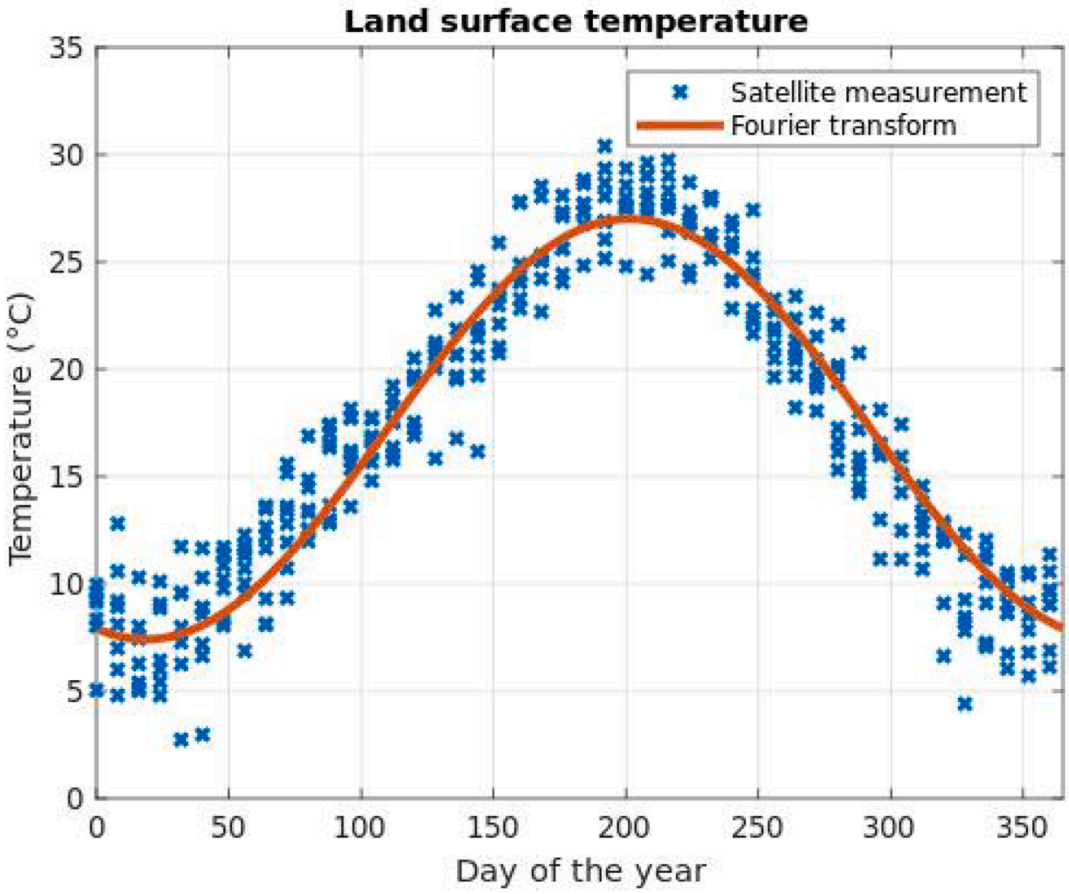

Fig. 5. Satellites land surface temperature since 2009 and the approximation of the values calculated with a Fourier transform.

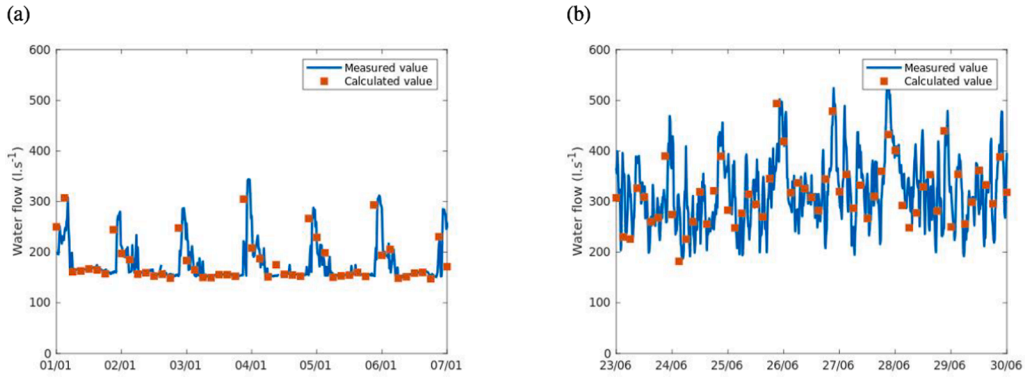

Fig. 6. Comparison between calculated and measured values for incoming water flow in January and June 2018.

$$Q_{in}(t) = \sum_{n} Q^{n}_{out}(t) \tag{27}$$

Fig. 6 shows the incoming water flow rate in January and June. During winter, the global demand is mainly due to industrial uses (measured with a flowmeter). During summer, consumption consists of industrial uses (same as in winter) and the more irregular watering uses. Small deviations between measurements and calculations come from the assumption that all the consumers have the same profile of consumption.

The water flow into the network is shown in Fig. 2. Water enters the network through two inlet points situated on the west of the network. Water is distributed through two connected main pipes and then to delivery points through many smallest pipes. Water flow in the system can vary rapidly with significant differences in value up to $100 l.s^{-1}$ in the main pipes of the water system.

3.2. Soil temperature measurement

The soil temperature measurement on the probe that is five meters horizontally from the pipe is used to evaluate the thermal diffusivity. The heat equation is solved by a finite difference method. Temperature measurement at the soil surface is used as an upper boundary condition. The root mean square error on soil temperature at 80 cm depth is minimized by adapting the soil thermal diffusivity. The minimum error (root mean square error on all measuring point) is obtained for a soil thermal diffusivity of eq. (28). Soil temperature at 80 cm depth for this value of diffusivity is shown in Fig. 7. The calculated value is very close to the measured one (the curves are overlapping on a large part of the

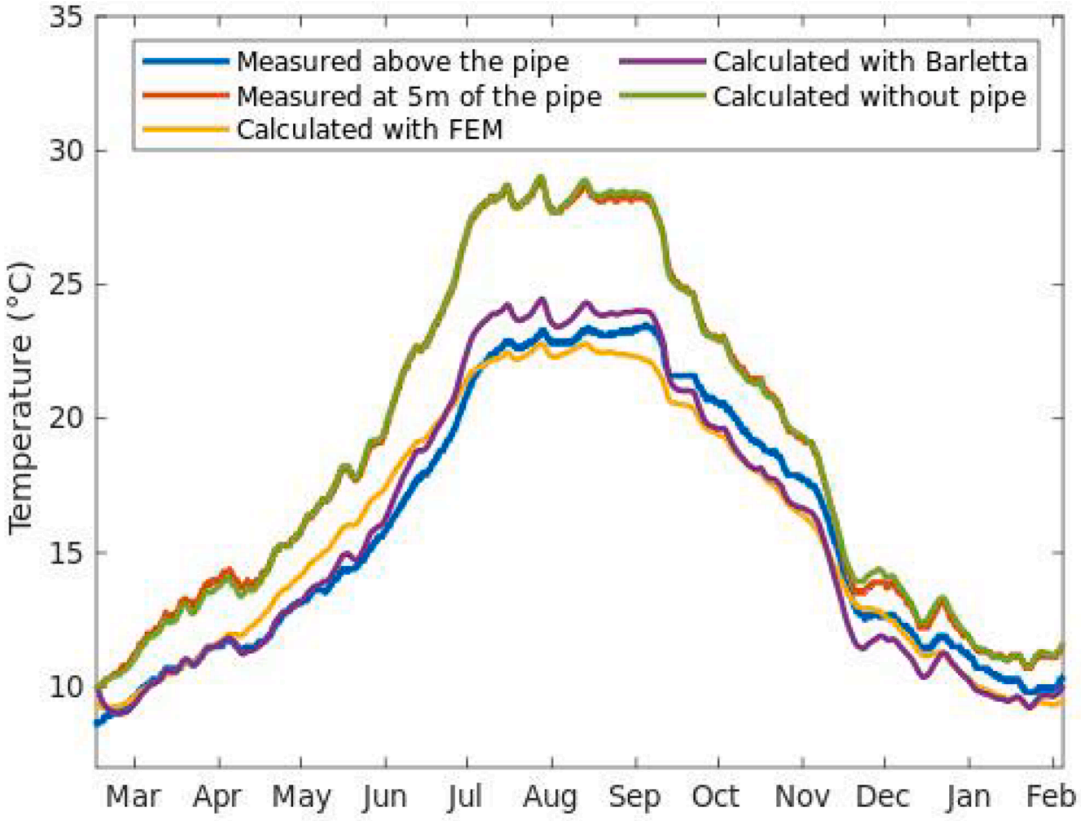

Fig. 7. soil temperature at 80 cm depth: measured values at 5 m of the pipe; calculted without pipe; measured values above the pipe; calculated values with imposed water temperature; calculated values with specified rate of heat transfer (calculated with Barletta's method).

Table 1
Parameters for heat transfer calculations.

	Symbol	Value	Unit
Pipe diameter	D_{in}	200	mm
Water Temperature	T_w	15	$°C$
Water velocity	v	1	$m.s^{-1}$
Soil thermal diffusivity	α_{soil}	$7{\cdot}10^{-7}$	$m^2.s^{-1}$
Mean temperature	T_m	17.26	$°C$
Amplitude	A_m	9.8	$°C$
Angular frequency	ω	$1.991{\cdot}10^{-7}$	$rad.s^{-1}$
Phase difference	Φ	2.82	–
Inlet temperature	T_{in}	18	$°C$
Pipe depth	z	1.1	m
Pipe conductivity	λ_{pipe}	46	$W.m^{-1}.K^{-1}$
Dimensionless burying depth	σ	11	–
Dimensionless angular frequency	Ω	$1.81{\cdot}10^{-3}$	–
Parameter A of Barletta's method	A	−0.7312	–
Parameter B of Barletta's method	B	0.1793	–

year).

$$\alpha_{soil} = 7{\cdot}10^{-7} m^2.s^{-1} \tag{28}$$

For a soil diffusivity between $5{\cdot}10^{-7}$ and $1.2{\cdot}10^{-6} m^2.s^{-1}$, the root mean square error on soil temperature at 80 cm is below $0.5°C$. These values are in agreement with typical values for soil thermal diffusivity [27,30,31].

The soil temperature measured above the pipe is compared with the calculated values. The method for the calculation is described in paragraph Section 2.1.2.4. The pipe boundary condition is either the measured water temperature or the rate of heat transfer calculated with Barletta's method [14]. Results obtained for the two types of boundary conditions and measured values are shown in Fig. 7. The good agreement shows that Barletta's method [14] can be used for water temperature calculation. It can also be noticed the important influence of the presence of the pipe. The maximum soil temperature at 80 cm deep is $5°C$ lower above the pipe than 5 m away.

3.3. Thermal model

The heat transfer between the soil and a pipe has been computed for the different models, according to Eqs. (4), (12), (16), (19), and (25). The parameters are shown in Table 1 and results in Fig. 8. The undisturbed soil model is excluded from Fig. 8 as it values are about 100 times higher than with other methods (this result is in agreement with [6]). For that reason, the impact of the soil cannot be neglected in the heat flux calculation.

Fig. 8 shows the difference of value from a finite element method with values from the shape factor model, Krarti Kreider's model, and Barletta's method. The method of Barletta et al. gives the same result as the finite element method, which was expected as the Barletta's is a reformulation of the finite element method. The benefit of this method is that it reduces the calculation time and the result can be obtained from tabulated parameters. Krarti kreider's overestimates the absolute value of heat transfer by up to 30%. The error can be explain as the model is out of its hypothesis as already mentionned in paragraph Section 2.1.2.3, that is here verified and computed.

For a pipe with a constant inlet temperature (T_{in}) and a constant flow rate ($\dot{m}$), the energy balance on the pipe is given in eq. (29). Therefore, the water temperature can be calculated with eq. (30).

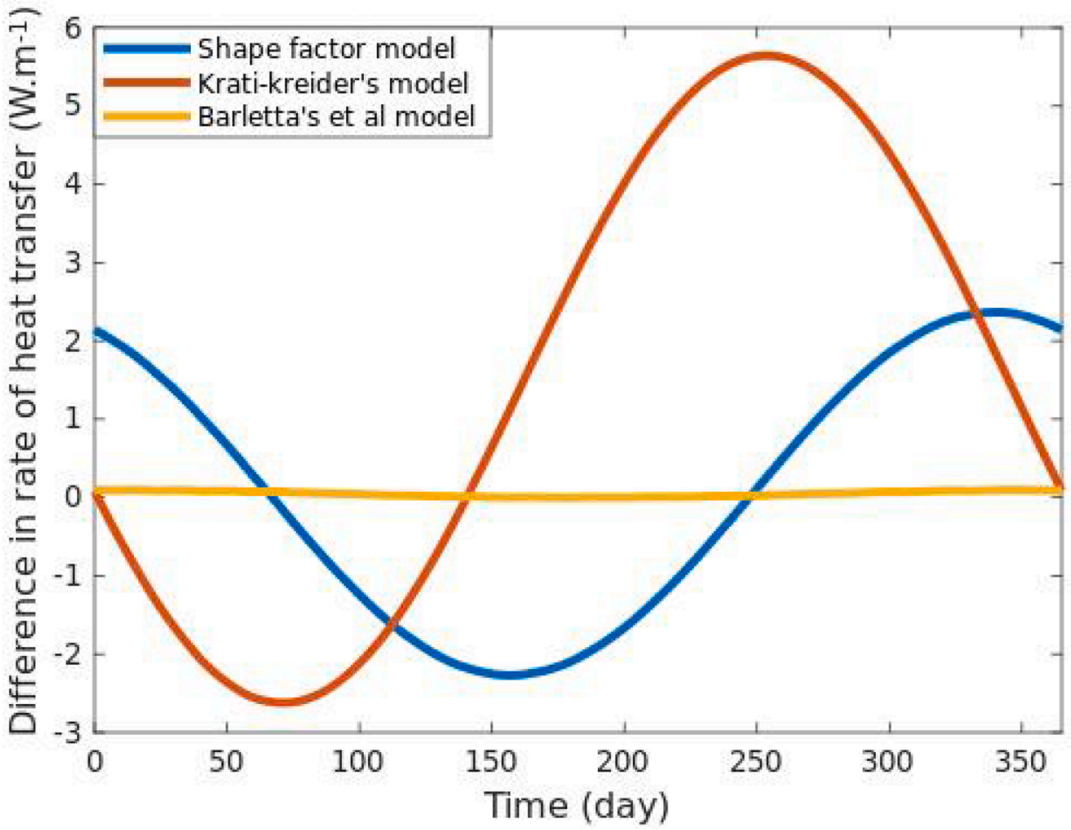

Fig. 8. Difference in heat flux calculated with models and with finite element method. The parameters used for calculation are presented in Tab.le 1.

$$\frac{d(T_\infty - T_w)}{dx} + \frac{T_\infty - Tw}{\dot{m}CpR_{tot}} = 0 \tag{29}$$

$$T_w = T_\infty - (T_\infty - T_{in}) \cdot \exp\left(\frac{-x}{\dot{m}CpR_{tot}}\right) \tag{30}$$

Water temperature obtained with eq. (30) for the different models are compared in Fig. 9. The calculation is made considering an inlet temperature of $T_{in} = 15°C$ on the 30th of June ($T_{surf} = 26.47°C$). With the undisturbed soil model, the water reaches the thermal equilibrium with the ground after about 400 m, whereas with the other models, it takes about 200 km. The different models do not use the same temperature to calculate the heat transfer. As a result, even if the thermal resistances are of the same order of magnitude, the choice of the model has a strong impact on the calculated water temperature. The use of shape factor model leads to an important error on the equilibrium temperature, as the reference temperature (T_∞) is the surface temperature. The error on equilibrium temperature is up to $5°C$.

Finally, because of its ability to describe the heat flux as well as the reference temperature (T_∞), Barletta's method is used.

Since the convection thermal resistance is small compared to the total thermal resistance (about 1000 time lower), the water velocity impact on the heat flux is small (less than 1%). But as the water temperature depends on the mass flow in the pipe, the impact of velocity on the water temperature is important. The length of pipe needed to reach a given temperature linearly depends on the water velocity. Indeed, if the thermal resistance does not depend on the water velocity ($R_{conv} \ll R_{tot}$), then the length (L) needed to reach a given temperature T_g between T_{in} and T_∞ is given in eq. (31) from eq. (30).

$$L = -v \cdot \frac{\pi D_{in}^2}{4} \cdot \rho \cdot Cp \cdot R_{tot} \cdot \ln\left(\frac{T_\infty - T_g}{T_\infty - T_{in}}\right) \tag{31}$$

The pipe diameter has a strong influence on the rate of heat transfer as the contact surface increases with it. For a given velocity, the water mass flow increases with the square of the diameter. As a result, the length of pipe to reach a thermal equilibrium also increases with the square of pipe diameter (eq. (31)).

3.4. Water system temperature

The heat exchange on the network has been solved according to (eq. (7), (8), (16), (24), and (26)). The calculation time with a cpu intel® Xeon(R) W-2135 CPU @3.70 GHz is 31 min.

3.4.1. Validation of the model

The result of the hydraulic calculation (see Section 3.1) is used as an input parameter for the thermal calculation. The inlet temperatures on the network are known and are specified as a boundary condition. The calculated values are compared to the measured ones at the points M1 to M3 of Fig. 2. Fig. 10 indicates the temperature and the flow for three points of the network during the year 2018. The difference in water flow profile between the three points is characteristic of the profiles that can be encountered. For M1 (Fig. 10(a)), the water flow is high and fluctuating (the base value is $40l.s^{-1}$). For M2 (Fig. 10(b)) the flow is small (between $2l.s^{-1}$ and $5l.s^{-1}$) and some rare peaks of $50l.s^{-1}$ can be observed. For M3 (Fig. 10(c)), flow is highly fluctuating between $0l.s^{-1}$ and $60l.s^{-1}$, with short time flow calls (with a typical value of one hour between two flow calls). The aspect of flow charts is due to the fluctuation of flow that leads to the overlapping of the curves.

The calculated water temperature matches the measured value for the three points (Fig. 11, $r^2 = 0.98$). The root mean square error on the modeled values is $0.84°C$. Therefore, the model can take into account the variability of flow according to time. As the points M1 and M2 are $1.5km$ apart, the temperature is almost the same.

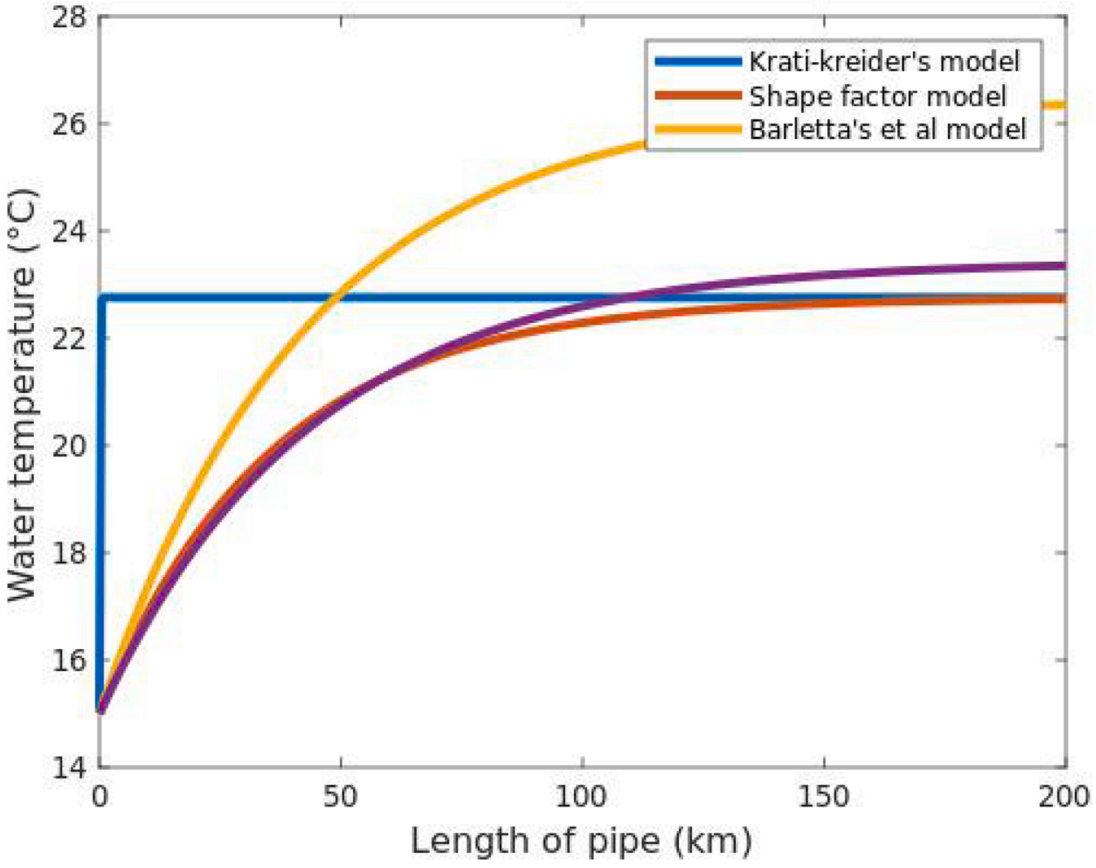

Fig. 9. water temperature along a pipe on June 30th, comparison between the different models. The parameters used for the calculation are presented in Tab.le 1.

3.4.2. Water system behavior

The water temperature profile on the network on June 30th at midday is shown in Fig. 12. The water temperature mainly depends on the season with a variation of about $10°C$ between the 30th of June and the 31st of December. Water temperature is almost independent of the time of day (maximum variation of $1°C$).

Water temperature in main pipes, (see Fig. 2), is close to inlet water temperature. On the contrary, in final pipes with higher residence time, water temperature is close to the soil temperature. It can be explained because the pipes are smaller and the speed in these pipes is lower. It is the two factors that increase the length to reach thermal equilibrium between pipes and soil (section 3.3).

3.4.3. Sensitivity analysis

The sensitivity of water temperature to input parameters has been studied.

The impact of amplitude (A_m) and mean value (T_m) of LST are studied (eq. (20)). Fig. 13 shows the impact of mean land surface temperature T_m ($10°C; 15°C; 20°C$) on water temperature at point M3. For each point on the network, increasing mean LST leads to an offset on the water temperature. As the water temperature depends on both inlet temperature and heat transfer, the temperature offset depends on the distance from the inlet points (E.g. for M3, $0.15°C/°C$).

Results for LST amplitude are similar to those obtained for mean LST: amplitude of water temperature increases with LST amplitude but the mean value of water temperature remains constant. For each point on the network, the amplitude linearly depends on LST amplitude(E.g. for M3 the impact is $0.25°C/°C$). Finally, as the variations of soil temperature are absorbed with depth, LST has a small impact on water temperature.

The model sensitivity to soil thermal conductivity is studied on Fig. 14. Heat exchange between pipes and soil is proportional to soil thermal conductivity (see eq. (25)). For high conductivity values, water temperature is strongly influenced by soil temperature. For small conductivity values, water temperature is slightly influenced by soil temperature and remains close to inlet water temperature. The impact of soil thermal diffusivity has also been studied. As described in eq. (10) the value of soil thermal diffusivity impacts soil temperature amplitude and phase differences. For thermal diffusivity between $2{\cdot}10^{-7}m^2.s^{-1}$ and $2{\cdot}10^{-6}m^2.s^{-1}$ the maximum deviation is $2°C$.

4. Application: impact of heat exchange on the network

The model is able to take into account the addition of heat exchanges on the network. The source term in eq. (2) is specified for given nodes. The water temperature after heat exchange T_h is given by (32).

$$T_h = T_0 + \frac{S}{\dot{m}Cp} \tag{32}$$

With T_0 the water temperature before heat exchange.

Some of the applications that can be considered are datacenter cooling, large compressor cooling, district heating networks or heating and cooling in industry.

For heating purposes, the network is use as a heat source and the source term is negative $S < 0$. Therefore, according to eq. (32) the water temperature decreases during the heat exchange. For cooling purposes, the network is use as a heat sink and the source term is positive $S > 0$. The temperature increases during the heat exchange.

The model that has been developed is able to take into account positive or negative source term. As an example, a positive source term of $2MW$ is added to the network (Fig. 15). The increase of temperature at this point is around $3°C$ (depending on the water flow). The temperature increases downstream the heat injection point. After this point, the

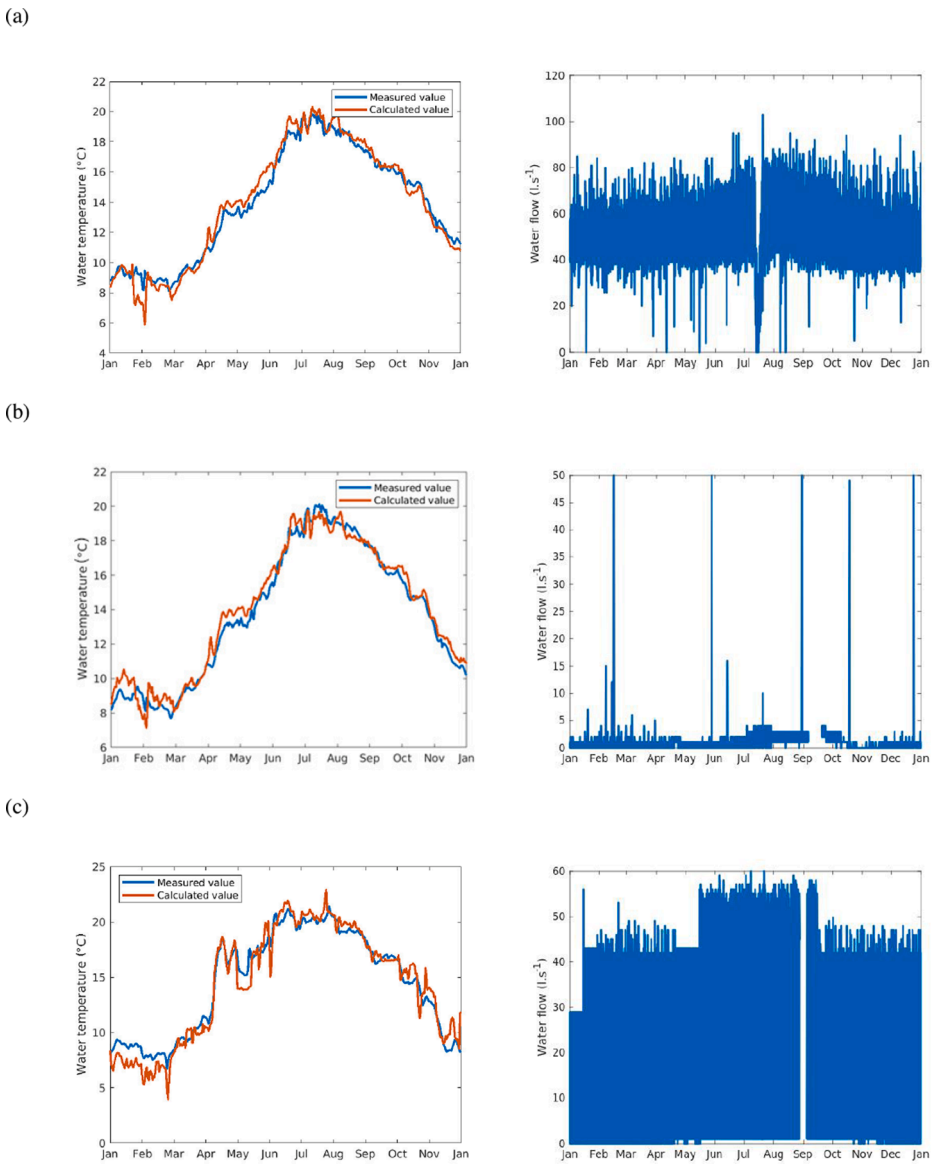

Fig. 10. water temperature (measured and calculated value) and water flow (measured value) during year 2018 for measurement points: (a) M1; (b) M2; (c) M3 (see Fig.. 2).

exchange between soil and pipe tends to bring the temperature back to the initial value. The influence is seen in the main pipe over a long distance, the water is heated by at least $1°C$ for 10 km downstream the exchange. Indeed, these pipes have a large diameter ($d = 500mm$), and the length to reach a given temperature depends on the square of the diameter (as described by eq. (31)). In smaller pipes, water reach soil temperature before the delivery points.

Similar calculation can be done for using the water network as a heat source by specifying negative source term. The water temperature decreased after the exchange. As before, the influence can be seen for a long distance in the main pipes.

5. Conclusion

The finding of this work is mainly to propose a dynamic model that describes the thermal behavior of large water systems. The model can predict the evolution of water temperature in every pipe of an extended water system during the year. The temperature in a large raw water network has been studied under steady periodic conditions. The transient heat transfer between the pipe and the surrounding soil is calculated. For that purpose, a method, initially developed in the petroleum industry to compute temperature in single pipes, has been applied to extended water systems. The direct solving for differentials equations has been implemented to speed-up calculation.

The novelty is also the use of satellite measurement for land surface temperature evaluation, the value is used as an upper boundary condition. Measurements have been performed to validate the satellites values. These values are readily available in all places. They can be used to replace a complete energy balance at the soil surface.

The model can be used to determine the temperature in different water systems (such as drinking water networks) for extended periods of time. As satellite measurements are available in all places, water systems in other locations can be modeled.

This model allows the calculation of heat exchange on water networks. They represent a large amount of water that can be used for district heating or cooling purposes. In this case, the last result shows that it is possible to ensure that the upper and lower limits for water temperature are not reached.

The work that will follow this study will be based on the heat potential calculation of the entire network. For this purpose, the heat

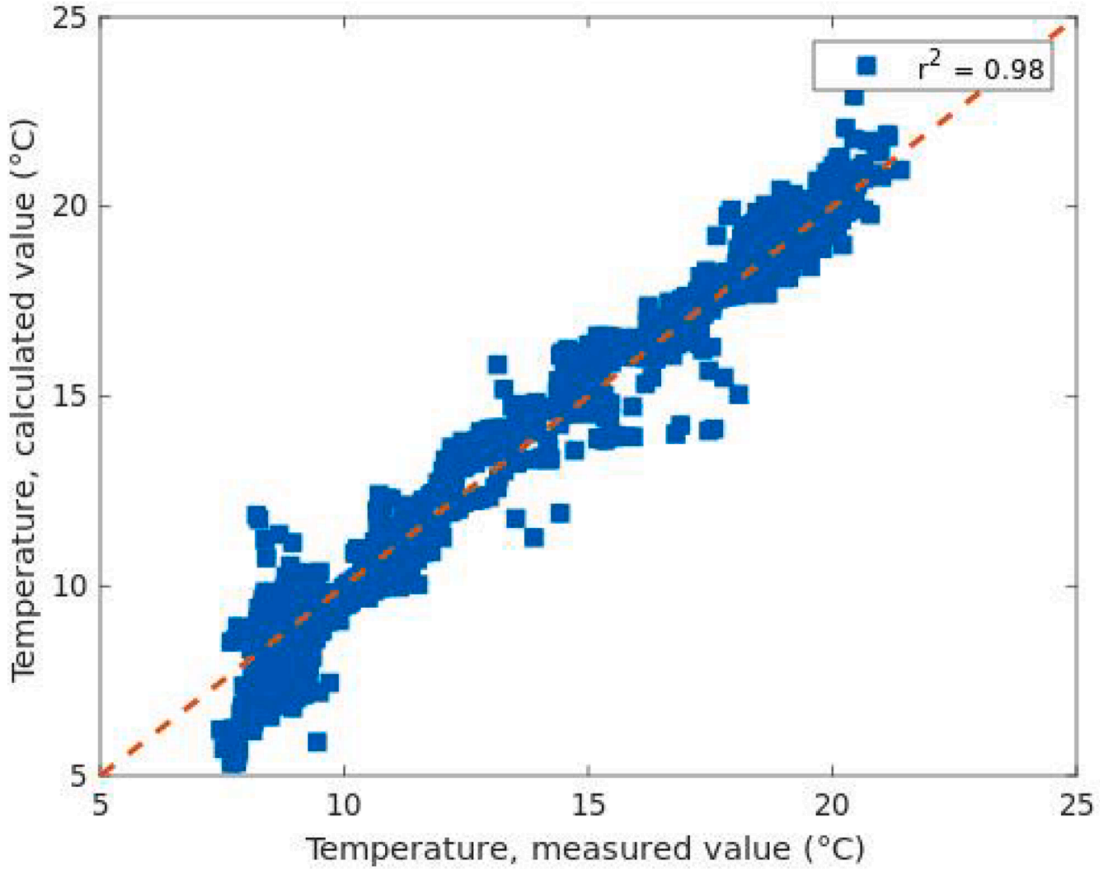

Fig. 11. Comparison between measured and calculated water temperature for year 2018 for points M1, M2 and M3.

Fig. 12. Modeled water temperature in the raw water network (presented in 2) on the 30th of June 2018 at midday (soil temperature is .21.6°*C*).

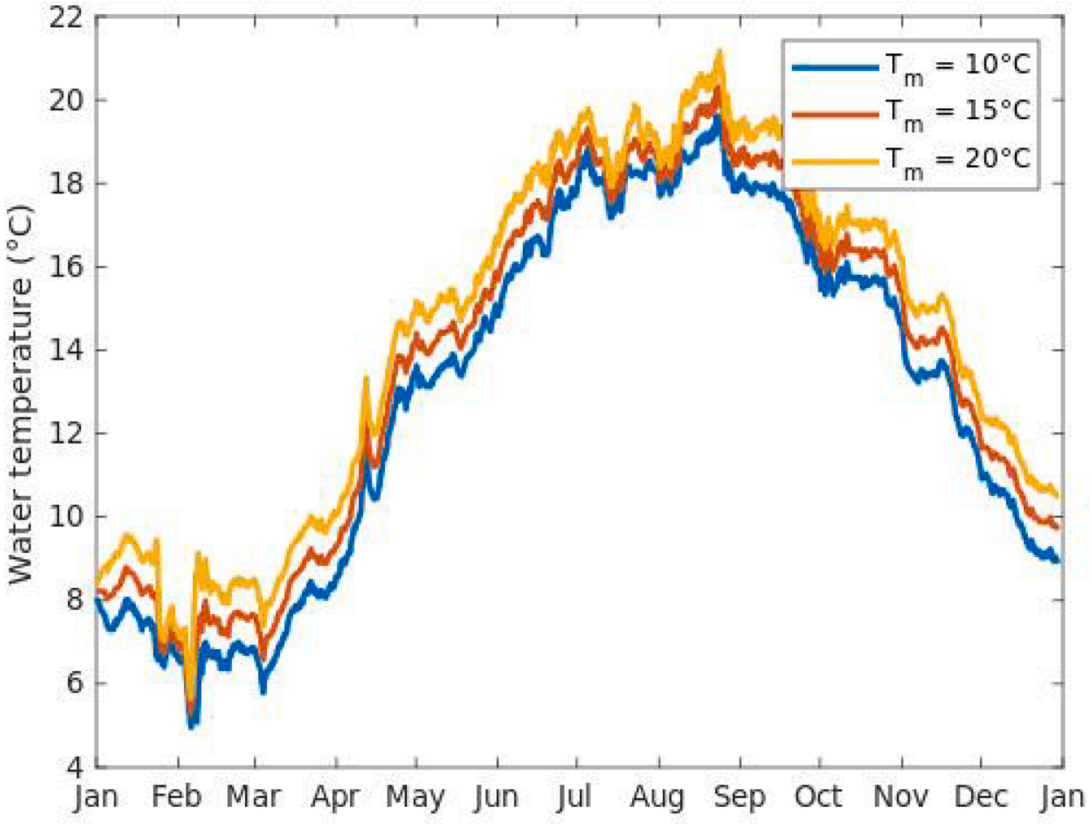

Fig. 13. impact of LST mean value on water temperature.

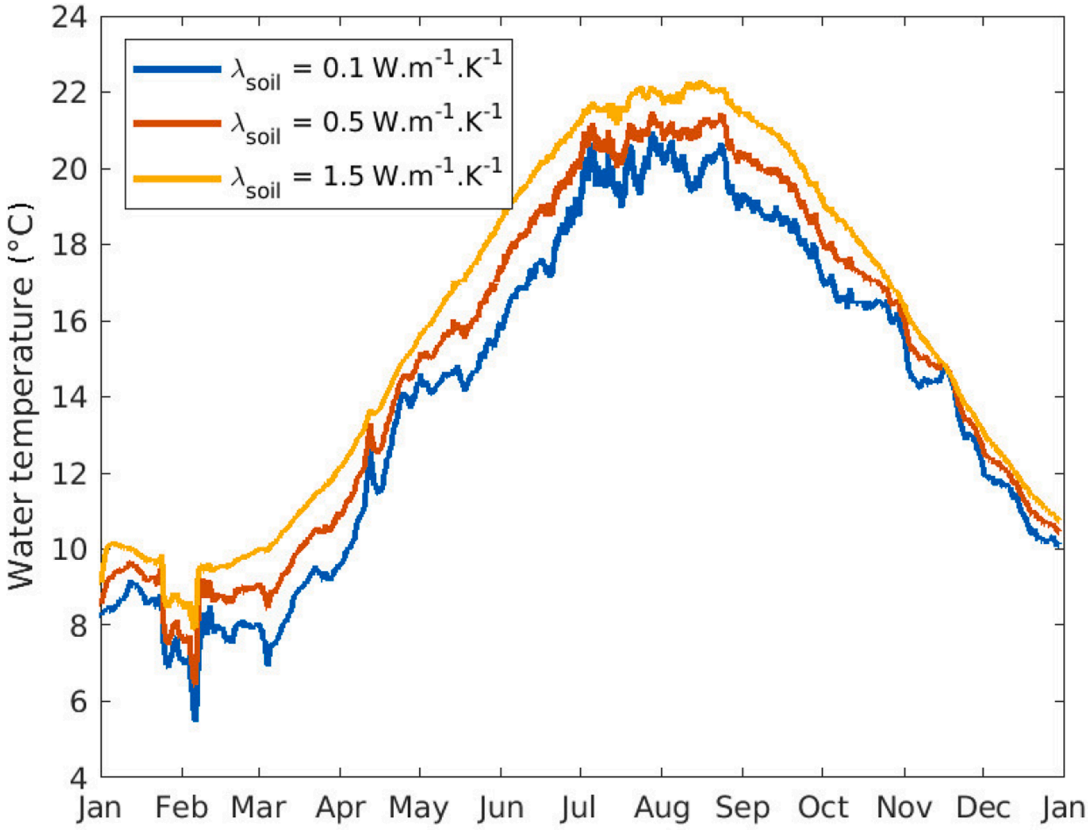

Fig. 14. Impact of soil thermal conductivity on water temperature (constant thermal diffusivity $\alpha_{soil} = 7{\cdot}10^{-7} m^2.s^{-1}$).

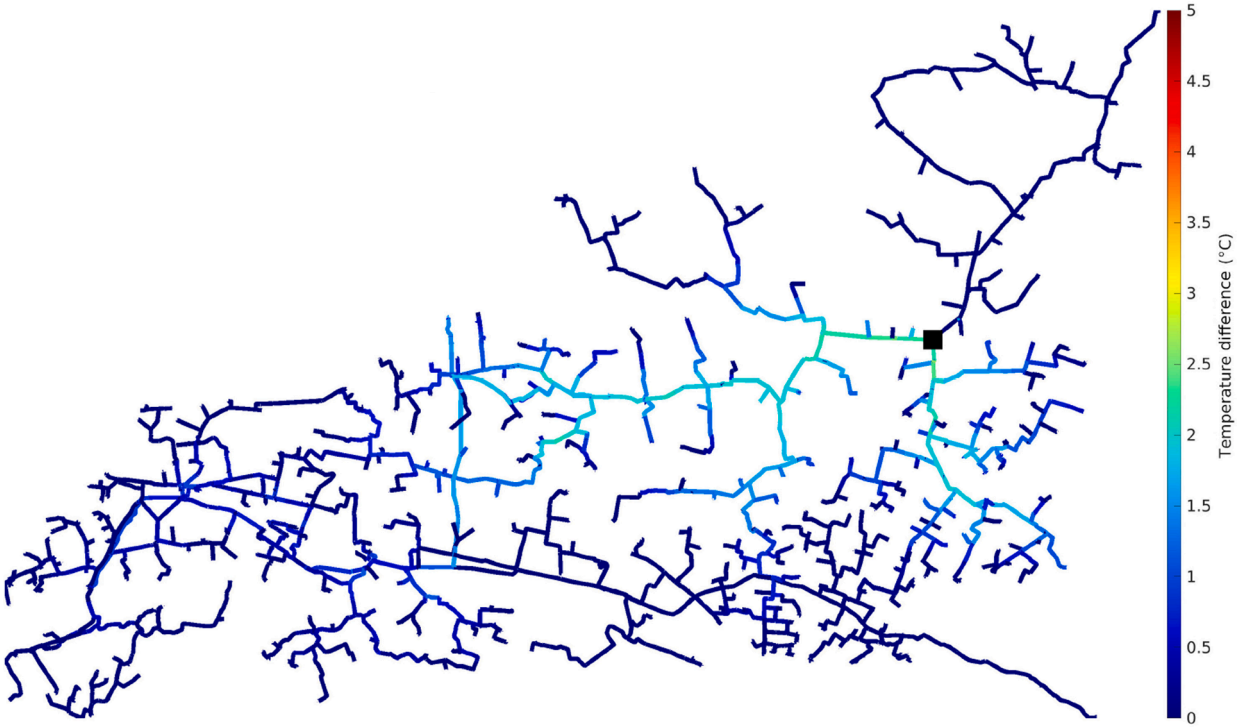

Fig. 15. modeled water temperature with a heat exchange on the 30th of June 2018 at midday difference with the reference value presented in Fig. 12. Heat exchange is represent by. a black square.

exchangersoptmal placement must be identified. Another issue that emerges from this study concerns the sizing of exchange systems in agreement with the dynamic aspect of the source temperature and flow.

Declaration of Competing Interest

The authors declare that they have no known competing financial interests or personal relationships that could have appeared to influence the work reported in this paper.

6. Appendix: Method of Barletta et al.

The first problem is to solve the heat equation in a plane orthogonal to the pipe. The temperature on the soil surface is given with a sine function, the vertical and bottom boundary (far from the pipe) are adiabatic. Coordinates in the initial plane are x and y. Barletta et al. [14] give a method to calculate the heat flux between the pipe and the surrounding soil. The value of the heat flux is given by eq. (20) and requires the calculation of two parameters A and B that are given by eq. (33) and (34).

$$A = \frac{1}{\Lambda_0} \int_{\partial L^*} \vec{n} \cdot \overrightarrow{\nabla^* \theta_1 dl} \tag{33}$$

$$B = \frac{1}{\Lambda_0} \int_{\partial L^*} \vec{n} \cdot \overrightarrow{\nabla^* \theta_2 dl} \tag{34}$$

Where variables θ_1 and θ_2 are the solutions to the problem (35).

$$\nabla^{*2} \theta_1 = -\Omega \theta_2 \tag{35}$$

$$\nabla^{*2} \theta_2 = -\Omega \theta_1 \tag{36}$$

With the boundary condition:

$$\begin{aligned} \theta_1 = 0; \theta_2 = 0 \quad & \text{On the pipe surface} \\ \theta_1 = 1; \theta_2 = 0 \quad & \text{On the surface} \\ \vec{n} \cdot \vec{\nabla}^* \theta_1 = 0; \vec{n} \cdot \vec{\nabla}^* \theta_2 = 0 \quad & \text{On the vertical and bottom sides} \end{aligned}$$

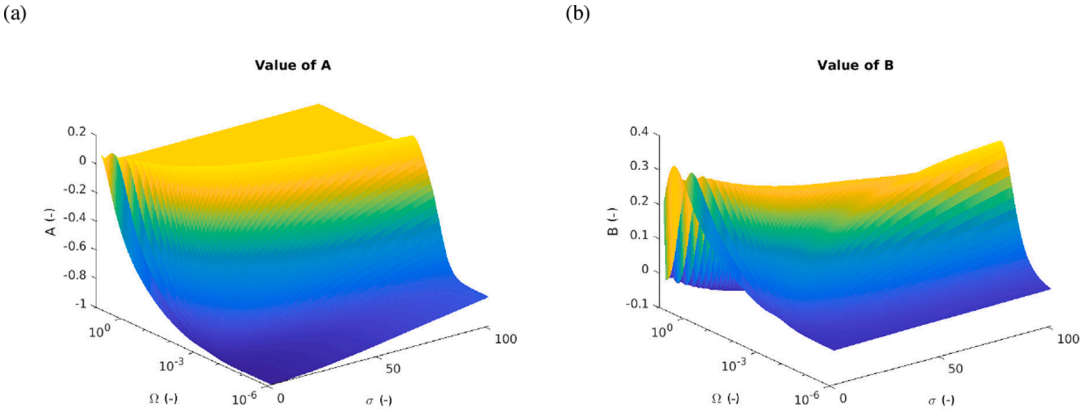

Fig. 16. Value of parameter A and B of Barletta's method [14] according to Ω. and σ.

Where the subscript $*$ denotes the dimensionless domain where the coordinates are $x^* = x/r$ and $y^* = y/r$ (r is the pipe radius) and the pipe center has the coordinates $[0, 0]$.

∂L^* is the boundary of the duct in the dimensionless domain; $\vec{n}$ is the vector normal to ∂L^*.

Contrary to the initial problem, the system (35) is steady, it is solved with a finite element method using Matlab (createpde function). The computational domain used for the calculation is similar as the one of Fig. 1. Then parameters A and B are obtained by integration of the gradient of θ_1 and θ_2 on the pipe surface using a trapezoidal numerical integration. The values obtained by [14] are recalculated to validate the method. A maximum difference of the order of 10^{-4} is obtained. The values for A and B according to Ω and σ are given in Fig. 16.

Declaration of Competing Interest

The authors declare that they have no known competing financial interests or personal relationships that could have appeared to influence the work reported in this paper.

Appendix A. Supplementary material

Supplementary data to this article can be found online at https://doi.org/10.1016/j.applthermaleng.2021.117261.

References

[1] B. Bach, J. Werling, T. Ommen, M. Münster, J.M. Morales, B. Elmegaard, Integration of large-scale heat pumps in the district heating systems of Greater Copenhagen, Energy 107 (2016) 321–334, https://doi.org/10.1016/j.energy.2016.04.029.

[2] Société du Canal de Provence, http://www.canal-de-provence.com/Accueil/tabid/36/language/fr-FR/Default.aspx (2020).

[3] J.P. van der Hoek, S. Mol, S. Giorgi, J.I. Ahmad, G. Liu, G. Medema, Energy recovery from the water cycle: Thermal energy from drinking water, Energy 162 (2018) 977–987, https://doi.org/10.1016/j.energy.2018.08.097.

[4] M. Blokker, A.M. van Osch, R. Hogeveen, C. Mudde, Thermal energy from drinking water and cost benefit analysis for an entire city, Journal of Water and Climate Change 4 (1) (2013) 11–16, https://doi.org/10.2166/wcc.2013.010.

[5] J. Piotr, N. Elżbieta, Water pipe network as a heat source for heat pump integrated into a district heating, E3S Web of Conferences 22 (2017) 00210.

[6] A.M. De Pasquale, A. Giostri, M.C. Romano, P. Chiesa, T. Demeco, S. Tani, District heating by drinking water heat pump: Modelling and energy analysis of a case study in the city of Milan, Energy 118 (2017) 246–263, https://doi.org/10.1016/j.energy.2016.12.014.

[7] H. Hubeck-Graudal, J.K. Kirstein, T. Ommen, M. Rygaard, B. Elmegaard, Drinking water supply as low-temperature source in the district heating system: A case study for the city of Copenhagen, Energy 194 (2020) 116773, https://doi.org/10.1016/j.energy.2019.116773.

[8] M. Blokker, E.J. Pieterse-Quirijns, Modeling temperature in the drinking water distribution system, Journal (American Water Works Association) 105 (1) (2013) E19–E28.

[9] A. Moerman, E.J.M. Blokker, J.H.G. Vreeburg, J.P. van der Hoek, Drinking Water Temperature Modelling in Domestic Systems, Procedia Engineering 89 (2014) 143–150, https://doi.org/10.1016/j.proeng.2014.11.170.

[10] C. Agudelo-Vera, M. Blokker, I. Pieterse-Quirijns, Early Warning Systems to Predict Temperature in the Drinking Water Distribution Network, Procedia Engineering 70 (2014) 23–30, https://doi.org/10.1016/j.proeng.2014.02.004.

[11] C. Agudelo-Vera, S. Avvedimento, J. Boxall, E. Creaco, H. de Kater, A. Di Nardo, A. Djukic, I. Douterelo, K.E. Fish, P.L. Iglesias Rey, N. Jacimovic, H.E. Jacobs, Z. Kapelan, J. Martinez Solano, C. Montoya Pachongo, O. Piller, C. Quintiliani, J. Ručka, L. Tuhovčák, M. Blokker, Drinking Water Temperature around the Globe: Understanding, Policies, Challenges and Opportunities, Water 12 (4) (2020) 1049, https://doi.org/10.3390/w12041049.

[12] F.P. Incropera, D.P. DeWitt, T.L. Bergman, A.S. Lavine (Eds.), Principles of Heat and Mass Transfer, 7th Edition, Wiley, Singapore, 2013.

[13] M. Krarti, J.F. Kreider, Analytical model for heat transfer in an underground air tunnel, Energy Convers. Manage. 37 (10) (1996) 1561–1574, https://doi.org/10.1016/0196-8904(95)00208-1.

[14] A. Barletta, E. Zanchini, S. Lazzari, A. Terenzi, Numerical study of heat transfer from an offshore buried pipeline under steady-periodic thermal boundary conditions, Appl. Therm. Eng. 28 (10) (2008) 1168–1176, https://doi.org/10.1016/j.applthermaleng.2007.08.004.

[15] K. Wang, J.J. Zhang, B. Yu, J. Zhou, J.H. Qian, D.P. Qiu, Numerical Simulation on the Thermal and Hydraulic Behaviors of Batch Pipelining Crude Oils with Different Inlet Temperatures, Oil & Gas Science and Technology - Revue de l'IFP 64 (4) (2009) 503–520, https://doi.org/10.2516/ogst/2009015.

[16] A. Oosterkamp, T. Ytrehus, S.T. Galtung, Effect of the choice of boundary conditions on modelling ambient to soil heat transfer near a buried pipeline, Appl. Therm. Eng. 100 (2016) 367–377, https://doi.org/10.1016/j.applthermaleng.2016.01.057.

[17] A. Chervinsky, Y. Manheimer-Timnat, Transfer of liquefied natural gas in long insulated pipes, Cryogenics 9 (3) (1969) 180–185, https://doi.org/10.1016/0011-2275(69)90212-4.

[18] H.H. Bau, S. Sadhai, Heat losses from a fluid flowing in a buried pipe, Int. J. Heat Mass Transf. 25 (11) (1982) 1621–1629, https://doi.org/10.1016/0017-9310(82)90141-7.

[19] R.A. Archer, O&apos, M.J. Sullivan, Models for Heat Transfer from a Buried Pipe, SPE Journal 2 (02) (1997) 186–193, https://doi.org/10.2118/36763-PA.

[20] Z. Wan, S. Hook, G. Hulley, MOD11A1 MODIS/Terra Land Surface Temperature/Emissivity Daily L3 Global 1km SIN Grid V006 [Data set], NASA EOSDIS Land Processes DAACdoi:10.5067/MODIS/MOD11A1.006.

[21] Z. Wan, S. Hook, G. Hulley, MYD11A1 MODIS/Aqua Land Surface Temperature/Emissivity Daily L3 Global 1km SIN Grid V006 [Data set], NASA EOSDIS Land Processes DAACdoi:10.5067/MODIS/MYD11A1.006.

[22] K. Thome, Terra — The EOS Flagship, https://terra.nasa.gov/.

[23] L.A. Rossman, P.F. Boulos, Numerical Methods for Modeling Water Quality in Distribution Systems: A Comparison, Journal of Water Resources Planning and Management 122 (2) (1996) 137–146, https://doi.org/10.1061/(ASCE)0733-9496(1996)122:2(137).

[24] F. Shang, J.G. Uber, L.A. Rossman, EPANET multi-species extension user's manual, Risk Reduction Engineering Laboratory, US Environmental Protection Agency, Cincinnati, Ohio.

[25] L.A. Rossman, EPANET 2: Users manual.

[26] S.-B. Duan, Z.-L. Li, H. Li, F.-M. Göttsche, H. Wu, W. Zhao, P. Leng, X. Zhang, C. Coll, Validation of Collection 6 MODIS land surface temperature product using in situ measurements, Remote Sens. Environ. 225 (2019) 16–29, https://doi.org/10.1016/j.rse.2019.02.020.

[27] G. Hu, L. Zhao, X. Wu, R. Li, T. Wu, C. Xie, Y. Qiao, J. Shi, W. Li, G. Cheng, New Fourier-series-based analytical solution to the conduction–convection equation to calculate soil temperature, determine soil thermal properties, or estimate water flux, Int. J. Heat Mass Transf. 95 (2016) 815–823, https://doi.org/10.1016/j.ijheatmasstransfer.2015.11.078.

[28] J.E. Carson, Analysis of soil and air temperatures by Fourier techniques, J. Geophys. Res. 68 (8) (1963) 2217–2232.

[29] M. Badache, P. Eslami-Nejad, M. Ouzzane, Z. Aidoun, L. Lamarche, A new modeling approach for improved ground temperature profile determination, Renewable Energy 85 (2016) 436–444, https://doi.org/10.1016/j.renene.2015.06.020.

[30] J. Andújar Márquez, M. Martínez Bohórquez, S. Gómez Melgar, Ground Thermal Diffusivity Calculation by Direct Soil Temperature Measurement. Application to very Low Enthalpy Geothermal Energy Systems, Sensors 16 (3) (2016) 306, https://doi.org/10.3390/s16030306.

[31] D. Hillel, Environmental Soil Physics, Academic Press, San Diego, CA, 1998.